Materials Research Bulletin 70 (2015) 416–423

Contents lists available at ScienceDirect

Materials Research Bulletin

journal homepage: www.elsevier.com/locate/matresbu

Photoluminescence properties of cerium oxide nanoparticles as a function of lanthanum content

R.C. Deus [a], J.A. Cortés [a,*], M.A. Ramirez [a], M.A. Ponce [c], J. Andres [b], L.S.R. Rocha [a], E. Longo [b,1], A.Z. Simões [a,*]

[a] Universidade Estadual Paulista, Unesp —Faculdade de Engenharia de Guaratinguetá, Av. Dr Ariberto Pereira da Cunha 333, Bairro Pedregulho, P.O. Box 355, 12.516-410 Guaratinguetá, São Paulo, Brazil,

[b] Laboratório Interdisciplinar em Cerâmica, Instituto de Química, Universidade Estadual Paulista, P.O. Box 355, 14801-907 Araraquara, São Paulo, Brazil

[c] Instituto de Investigaciones en Ciencia y Tecnología de Materiales (INTEMA) (CONICET-Universidad Nacional de Mar del Plata), Juan B. Justo 4302, 7600 Mar del Plata, Argentina

ARTICLE INFO

Article history:
Received 5 February 2015
Received in revised form 29 April 2015
Accepted 4 May 2015
Available online 7 May 2015

Keywords:
Ceramics
Nanostructures
Crystal growth
X-ray diffraction
Luminescence

ABSTRACT

The structural and photoluminescent properties at room temperature of CeO_2 and La-doped CeO_2 particles were undertaken. The obtained particles were synthesized by a microwave-assisted hydrothermal method (MAH) under different lanthanum contents. X-ray diffraction (XRD), Fourier transform infrared (FT-IR), Fourier transform Raman (FT-Raman), Ultra-violet spectroscopy (UV–vis) and photoluminescence (PL) measurements were carried out. XRD revealed that the powders are free of secondary phases and crystallize in the cubic structure. Raman data show that increasing La doping content increase oxygen vacancies due to lattice expansion. The UV/vis absorption spectroscopy suggested the presence of intermediate energy levels in the band gap of structurally ordered powders. Lanthanum addition creates oxygen vacancies and shifts the photoluminescence in the low energy range leading to intense PL emission.

1. Introduction

Cerium dioxide (CeO_2, ceria) [1] is a technologically important ceramic material used in various fields in the past few years, such as gas sensors [2], fuel cells [3], polishing materials [4], phosphors [5], energy storage materials [6], catalysts [7–9] and for which the use of nanocrystalline powders is an important factor. Several methods have been developed to prepare ultrafine CeO_2 powder, including conventional hydrothermal [4,10], co-precipitation [4], polymeric precursor [11], flow method [12], organometallic decomposition [13], microwave-assisted heating [14]. In previous work our group has give strong efforts in the preparation of CeO_2 nanoparticles with microwave-hydrothermal methods. CeO_2 synthesized by MAH under NH_4OH revealed agglomerate particles while CeO_2 synthesized under MAH conditions on KOH and NaOH mineralizers agent were well-dispersed and homogeneously distributed. The CeO_2 sample has better crystallization in the treatment at 8 min. CeO_2 synthesized by MAH under lower soaking times revealed agglomerate particles while CeO_2 synthesized under MAH conditions on higher soaking times were well-dispersed and homogeneously distributed. This can be explained by the amount of hydrogen bonds during the drying and calcining process to hard agglomerates of particles. UV–vis spectra revealed the presence of localized energy levels into the band gap of CeO_2 powders with a soaking time of 4 and 8 min possibly due to the certain structural order degree in the lattice [15–16]. Recently, Zhang et al. [17] have been provided a comprehensive review of current research activities that focus on the shape-controlled synthesis methods of ceria nanostructures. Pure CeO_2 is a poor ionic conductor with a band gap of 6 eV [18] adopting the fluorite structure (space group Fm3m) with oxygen vacancies ($V_{\ddot{O}}$) as the predominant ionic defect, which have been identified as the main fact for storing oxygen in ceria, as its catalysis activity originates from its surface oxygen, related to the Ce/O ratio [19]. Ceria-based electrolytes have been extensively studied and made much progress. In particular, some singly doped-electrolytes can be obtained by doping the ceria host structure with other cations, such as $Ce_{1-x}Gd_xO_{2-\delta}$, $Ce_{1-x}Sm_xO_{2-\delta}$, $Ce_{1-x}Y_xO_{2-\delta}$, showing high oxide ion conductivity at intermediate temperatures (500–700 °C) [13,20–24]. Various rare-earth doped ceria (La, Sm, Pr) have successfully been prepared by hydrothermal treatment, providing low-temperature preparation and

* Corresponding authors. Tel.: +55 12 3123 2765; fax: +55 12 3123 2800.
E-mail addresses: leandrosrr89@gmail.com (J.A. Cortés), alezipo@yahoo.com (A.Z. Simões).
[1] Tel.: +55 16 3301 6643; fax: +55 16 3301 6692.

http://dx.doi.org/10.1016/j.materresbull.2015.05.006
0025-5408/

morphological control of ultrafine particles with uniform crystallite dimension [21,25–28]. The substitution of Ce^{4+} (r = 0.111 nm) by larger cations such as Gd^{3+} (r = 0.119 nm) [29–31] has been examined in great detail by a number of authors, and gadolinium-doped ceria is considered for being one of the best ceria-based solid electrolytes currently available [32]. In this paper, we have synthetized La-doped ceria by means of a microwave-assisted hydrothermal (MAH) method and the formation conditions of ceria are reported in detail, emphasizing the advantages of microwave irradiation. In addition, the photoluminescence properties of the as-prepared materials have been discussed [33].

The main goal of lanthanum addition will account of lower valence state of La^{3+} (r = 0.1032 nm) than Ce^{4+}, which will induce the production of more oxygen vacancies for charge balance, resulting in an improvement of the oxygen mobility [34].

2. Experimental procedure

CeO_2 powders were synthesized by a hydrothermal microwave route. Ammonium cerium (IV) nitrate (5×10^{-3} mol L^{-1} Ce $(NH_4)_2(NO_3)_6$, 99.9% purity) was dissolved in 80 ml of deionized water under constant stirring for 15 min at room temperature. La-doped CeO_2 ceramic powders were synthesized using the method of microwave assisted hydrothermal synthesis with values of x = 0.04, 0.08, and 0.12 mol%. The experimental procedure for preparation of La-doped CeO_2 based on dissolution of the ammonium cerium (IV) nitrate (purity 99%—Sigma) in an aqueous medium, followed by heating at 50 °C under constant agitation. Separately, lanthanum oxide (La_2O_3) (99% purity—Aldrich) was dissolved in a nitric acid medium and added to solution of Ce. The resulting mixture was heated at 70 °C under stirring and its pH adjusted through the addition of basic aqueous solution 2 mol L^{-1} of KOH (99.5% purity—Synth) until a pH ~ 10. The resulted solution was transferred into a sealed Teflon autoclave and placed in a hydrothermal microwave (2.45 GHz, maximum power of 800 W). The reactional system was heat treated at 100 °C with a soaking time of 8 min and a heating rate fixed at 10 °C/min. The pressure in the sealed autoclave was stabilized at 1.2 atm. The autoclave was cooled to the room temperature naturally. CeO_2 powders were centrifuged and washed with deionized water and then dried at 100 °C in an oven for 2 days. The obtained powders were characterized with X-ray powder diffraction (XRD) using a (Rigaku-DMax/2500PC, Japan) with Cu-Kα radiation (λ = 1.5406 Å) in the 2θ range from 20 to 75° with 0.2 0/min. The crystallite size (d) of CeO_2 was calculated using Scherrer equation $d = k\lambda/\beta \cos\theta$, where k is constant, λ is wavelength of X-rays and β is the full width at half maximum (FWHM) for (1 1 1) reflection measured from slow scan where θ is the diffraction angle of the main peak. For Rietveld analyses, X-ray diffraction data were collected under the following experimental conditions: 40 kV, 30 mA, $20° \leq 2\theta \leq 110$, $\Delta 2\theta = 0.02$ °, λCu Kα monocromatized by a graphite crystal, divergence slit = 2 mm, reception slit = 0.6 mm, step time = 10 s. The Rietveld analysis was performed with the Rietveld refinement program DBWS-941 1. The profile function used was the modified Thompson–Cox–Hasting pseudo-Voigt, in which η (the lorentzian fraction of the function) varies with the Gauss and Lorentz components of the full width at half maximum. Raman spectra were collected (Bruker RFS-100/S Raman spectrometer with Fourier transform). A 1064 nm YAG laser was used as the excitation source, and its power was kept at 150 mW. Ultraviolet–vis (UV–vis) spectroscopy for the optical absorbance spectra of CeO_2 powders was taken using Cary 5G equipment. Specimens for TEM were obtained by drying droplets of as-prepared samples from an ethanolic dispersion which had been sonicated for 5 min onto 300 mesh Cu grids. TEM images were then taken at an accelerating voltage of 200 kV on a Philips model CM 200 instrument. Photoluminescence (PL) properties were measured with a Thermal Jarrel-Ash Monospec 27 monochromator and a Hamamatsu R446 photomultiplier. The excitation source was 350.7 nm wavelength of a krypton ion laser (Coherent Innova) keeping their power at 200 mW. All measurements were taken at room temperature.

3. Results and discussion

Fig. 1 illustrates the X-ray diffraction of $Ce_{1-3/4x}La_xO_2$ particles (x = 0.00, 0.04, 0.08, and 0.12) obtained by the MAH at 100 °C for t = 8 min prepared with KOH. To provide the formation of solid solution we have carried out the partial replacement of Ce^{4+} ions with trivalent lanthanum till 0.12 concentration. It is know that rare earth doped ceria could create a corresponding number of anion vacancies and result in solid solution with high ionic conductivity and the defective surface of these materials may enhance their catalytic properties. Also, lanthanum can avoid the ceria crystallite growth in severe oxidizing environment as stabilizer. [35] XRD results confirmed that the CeO_2 powders doped exhibit similar to that of pure cerium oxide behavior. Analyzing the diffraction patterns (XRD) of the crystalline samples shown in Fig. 1, it is found that a widening of the peaks related to the crystallographic planes (1 1 1) and (2 2 0) at 2θ equal to 28° and 48° occurs, respectively due to incorporation of lanthanum in place of Ce, due to the change in crystallite upon insertion of rare-earth. It can be seen that the peaks are more intense in pure CeO_2 and decreases in intensity with increasing concentration of the lanthanum, and this behavior has been linked to "disturbance" of the crystalline structure when dopants are introduced [36]. The XRD patterns of as-prepared ceria powders showed the same crystalline structure for all the synthesis conditions used. All of the peaks can be well-indexed to a pure cubic structure of CeO_2 (space group: Fm3m) with lattice constant a = 5.411 Å, which is in good agreement with the JCPDS file for CeO_2 (JCPDS 34-394). The average crystallite sizes calculated by Debye Scherrer is around 3.2; 2.9, 4.80 and 5.10 nm at a La contents of 0.00; 0.04; 0.08 and 0.12 mol%, respectively. It is obvious that the amount of rare-earth changes the CeO_2 crystal growth. As the average diffusion distance for the diffusing solute is short and the concentration gradient is steep in concentrated solutions, much diffusing material passes per unit time through a unit area.

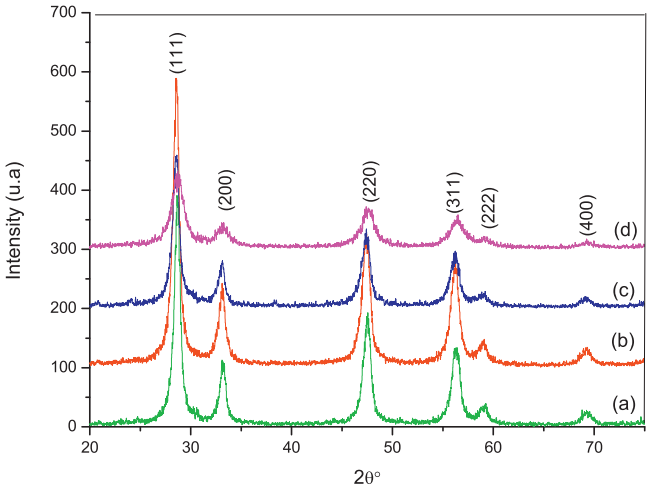

Fig. 1. (a) X-ray diffraction pattern of $Ce_{1-3/4x}La_xO_2$ nanoparticles synthesized at 100 °C in the MAH method under KOH mineralizer at different contents: (a) 0,00; (b) 0.04; (c) 0.08 and (d) 0.12.

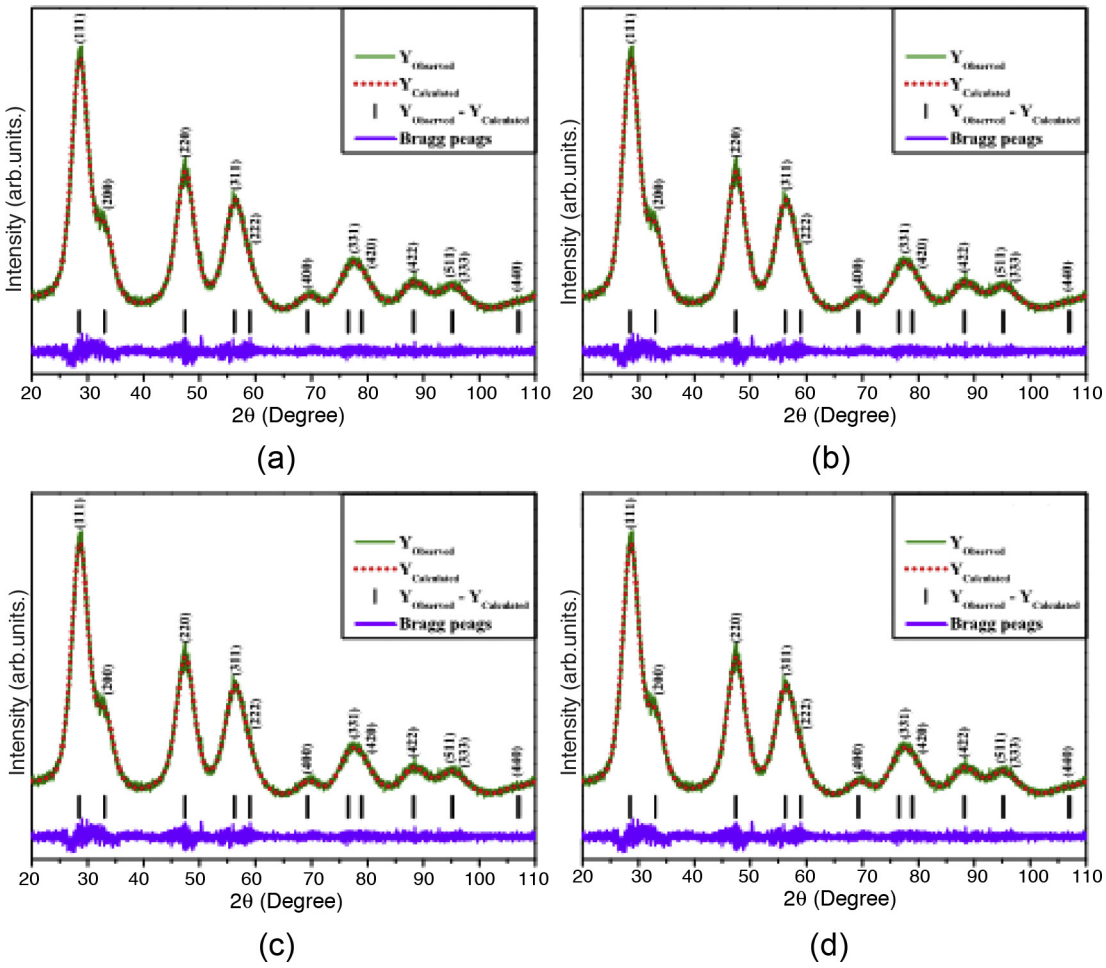

Fig. 2. Rietveld refinement of $Ce_{1-3/4x}La_xO_2$ nanoparticles synthesized at 100 °C in the MAH method under KOH mineralizer at different contents: (a) 0.00; (b) 0.04; (c) 0.08 and (d) 0.12.

Using the Rietveld refinement was possible to adjust the XRD patterns of the samples, as shown in Fig. 2. The lattice parameters, the unit cell volume and atomic positions for all the particles were obtained by Rietveld refinement [37] and calculated by means of the GSAS [38] software. It is observed that all samples showed reasonable values for the indices of refinement demonstrating that the refinement was successful because of the low distortion between theoretical and experimental curve. The La-doping process reduces the lattice parameter and the unit cell volume. Therefore, a redistribution of the charge density takes place (Fig. 3). Moreover, this change can be associated by the simple inclusion of lanthanum which has a greater radial stabilizing effect of oxygen vacancies and as a result the structure. The refinement of the oxygen vacancies indicates that atoms at positions O_2 and O_4 are contributing to vacancy formation. The refinement at positions O_1 and O_3 was unsuccessful once they are attached to cerium forming a square planar. The refinement of the atom in the O3 position was also not successful, because this binds oxygen atom to Ce_1, which has no vacancy, the fact that lanthanum is attached to it. Therefore, both the O_2 and O_4 atom positions contribute to the origin of vacancies, because the Ce_2, which presents vacancy, is free to migrate into the structure being composed of alternating layers of Ce_2, O_2 and O_4.

Fig. 4 confirm the formation of pure ceria by FT-Raman spectrum. Cubic fluorite structure-metal dioxides have a single Raman mode at 452.1 cm^{-1}, which has F2 g symmetry and can be viewed as a symmetric breathing mode of the O atoms around each cation. Since only the O atoms move, the vibrational mode is nearly independent of the cation mass [39,40]. As shown, three additional low intensity second scattering Raman bands are detected around 266, 598 and 726 cm^{-1}, respectively. These bands are usually assigned to the presence of extrinsic oxygen vacancies generated into the ceria lattice improving diffusion rate of bulk oxygen after lanthanum addition. The fast structural organization of CeO_2

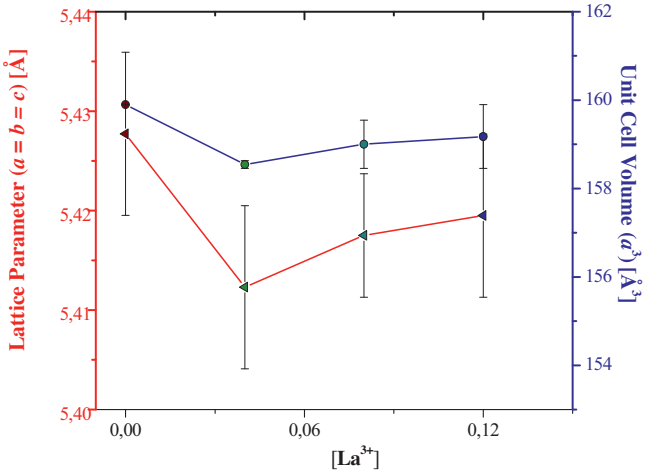

Fig. 3. Dependence of La content as a function of lattice parameter and unit cell volume.

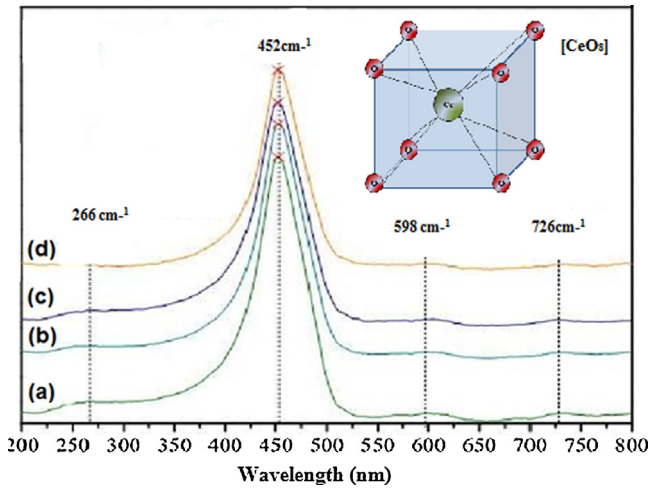

Fig. 4. Raman spectra of $Ce_{1-3/4x}La_xO_2$ nanoparticles synthesized at 100 °C in the MAH method under KOH mineralizer at different contents: (a) 0.00; (b) 0.04; (c) 0.08 and (d) 0.12.

particles processed in MAH can be related to the heating process which occurs from the interior to the surface. The microwave energy is transformed into heat through the interaction between molecules and atoms with the electromagnetic field. This interaction results in an internal and volumetric heating of the powders which promotes the formation of temperature gradients and heat flows. It is well known that the Raman signal is affected by these randomly oriented vacancies that distort long range ordering. The defect formation is a known source of structural disorder, and thus breakdown of translational symmetry occurs, which results in relaxation of the $k \cong 0$ selection rule for Raman scattering and hence phonons from all parts of the Brillouin zone contribute to the spectra. The measured Raman spectra exhibit a characteristic strong feature at $\cong 340–395\ cm^{-1}$. The position of this Raman band is related to the strength of the RE—O bond and for La_2O_3, extrapolating from other RE Raman data, can be expected to be at $\cong 370\ cm^{-1}$. Another broad weak band at $570\ cm^{-1}$ is considered to be attributed to oxygen vacancies [41–42]. With increasing La doping content, there is a small systemic broadening of band located at $452.1\ cm^{-1}$ which should be due to lattice expansion and an increase of oxygen vacancies

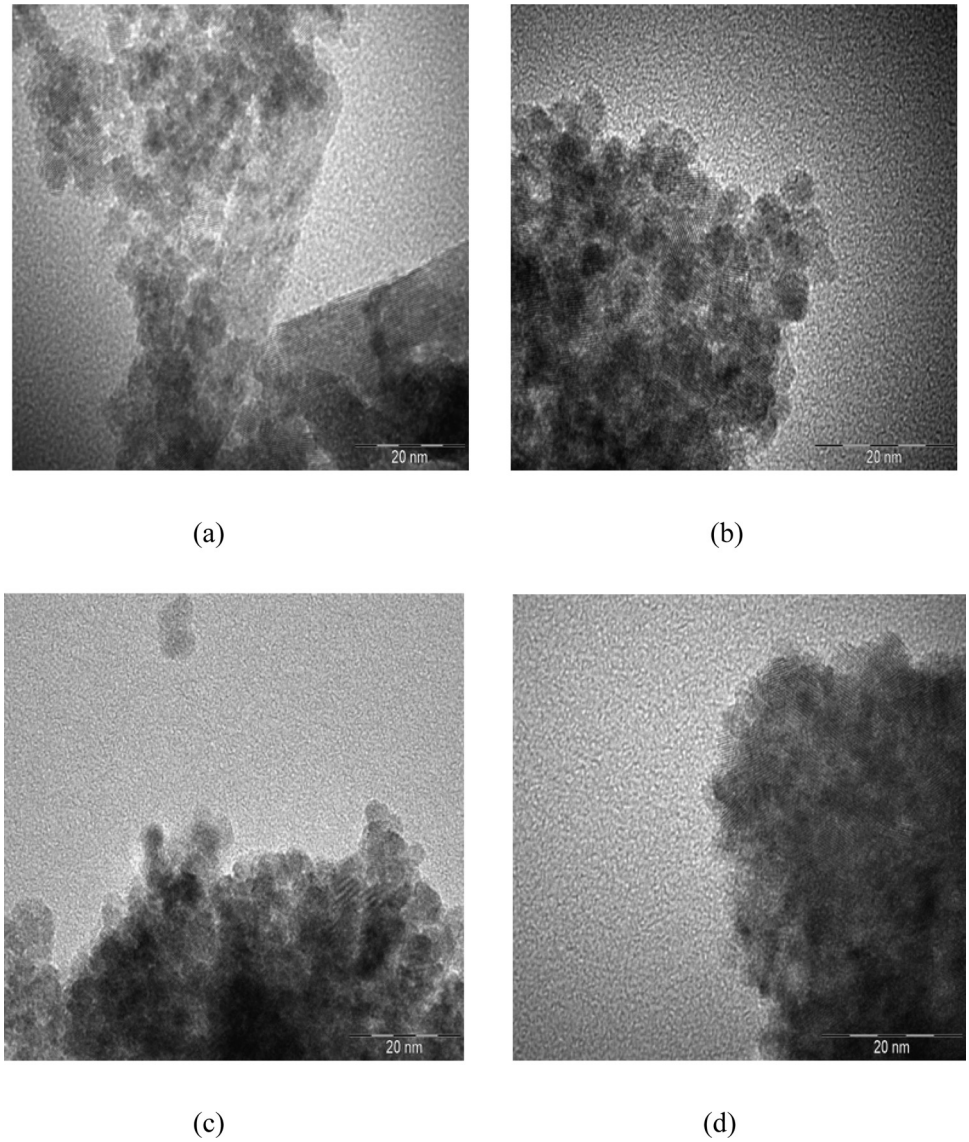

Fig. 5. TEM images of $Ce_{1-3/4x}La_xO_2$ nanoparticles synthesized at 100 °C in the MAH method under KOH mineralizer at different contents: (a) 0.00; (b) 0.04; (c) 0.08 and (d) 0.12.

[43]. This also indicates that La has incorporated into the ceria lattices to form Ce–La–O solid solution. In addition, the increase of A 570/A460 ratio (A570 and A460 are the peak areas at 570 cm^{-1} and 460 cm^{-1}, respectively) with increasing doping contents of La may reflect the increase of the oxygen vacancy concentration [44], that is, the oxygen vacancy concentration is increased after doping.

TEM micrographs of CeO_2 obtained at different La contents are shown in Fig. 5. CeO_2 synthesized by MAH under KOH at 100 °C for 8 min, revealed that particle sizes approximately range from 6 to 12 nm (Fig. 5a–d) with spherical shape. According to the image, most of the grains of CeO_2 nanoparticles are homogeneous with an average particle size of 6.7; 9.2; 10.4 and 12.1 nm as La content increases. Undoped CeO_2 powders obtained displays poor contrast and intense agglomeration amongst extremely fine particles. The small size of the CeO_2 particles synthesized by MAH can be explained quite simply. It is postulated that at the start of the reaction a large number of nucleus forms in the solution and as the reaction takes place in a very dilute solution there is not enough reactant left for the growth of the particles. As a result, the particles do not grow beyond 12 nm. The MAH process at KOH showed most effective to dehydrate the adsorbed water and decrease the hydrogen bonding effect leaving weakly agglomerated nanoparticles of hydrated ceria. Aggregation between the particles decreases and monodispersed particles are observed at higher La content. The higher agglomeration degree of undoped CeO_2 is due the Van der Waal's force derived for the —OH ligand precursor which was transformed to CeO_2 after hydrothermal treatment. Moreover, the distribution in size seemed to be homogeneous and the shape appeared rounded. The synthesized ceria particles were relatively spherical with uniform size distribution. Nanometric and isotropic CeO_2 crystallites obtained in this study are quite different from the previous study, where CeO_2 powders agglomerated into a cubic shape with the side size of 4.8 nm under hydrothermal conditions [45]. The images taken confirm the formation of nanocrystallites with uniform grain size and the absence of partial sintering or excessive growth of any nanocrystallites.

Fig. 6 illustrates the UV–vis spectral dependence of absorbance for the ordered CeO_2 particles. The maximum absorption was located at around 400 nm with respective band gap values determined from the Kubelka Model [46]. The opand to the photon energy by the following Eq. (1):

$$h\nu\alpha \propto (h^{\circ} - E_g{}^{opt})^2$$

where α is the absorbance, h is the Planck constant, ν is the frequency and $E_g{}^{opt}$ is the optical band gap [45]. The band gap was deduced by fitting the absorption data to the direct transition equation by extrapolating of the linear portions of the curves to absorption equal to zero. In structurally ordered CeO_2 particles, the absorbance measurements suggest a non uniform band gap structure with a tail of localized states (see Fig. 6a–d). The main changes in the optical band gap [E(gap)] energy can be correlated to the reduction of structural defects or localized states inside the band gap which decreases the intermediary energy levels at crystal structure. This behavior indicates that these samples present a certain structural order degree in agreement with the Raman spectra. The estimated band gaps were ranged between 2.81 and 3.00 eV. The uncertainty of these values was estimated at 0.05 eV. As La content increases, the optical band gap of the sample initially decreases and then increases because new levels of energy are formed promoting the appearance of intermediate electronic

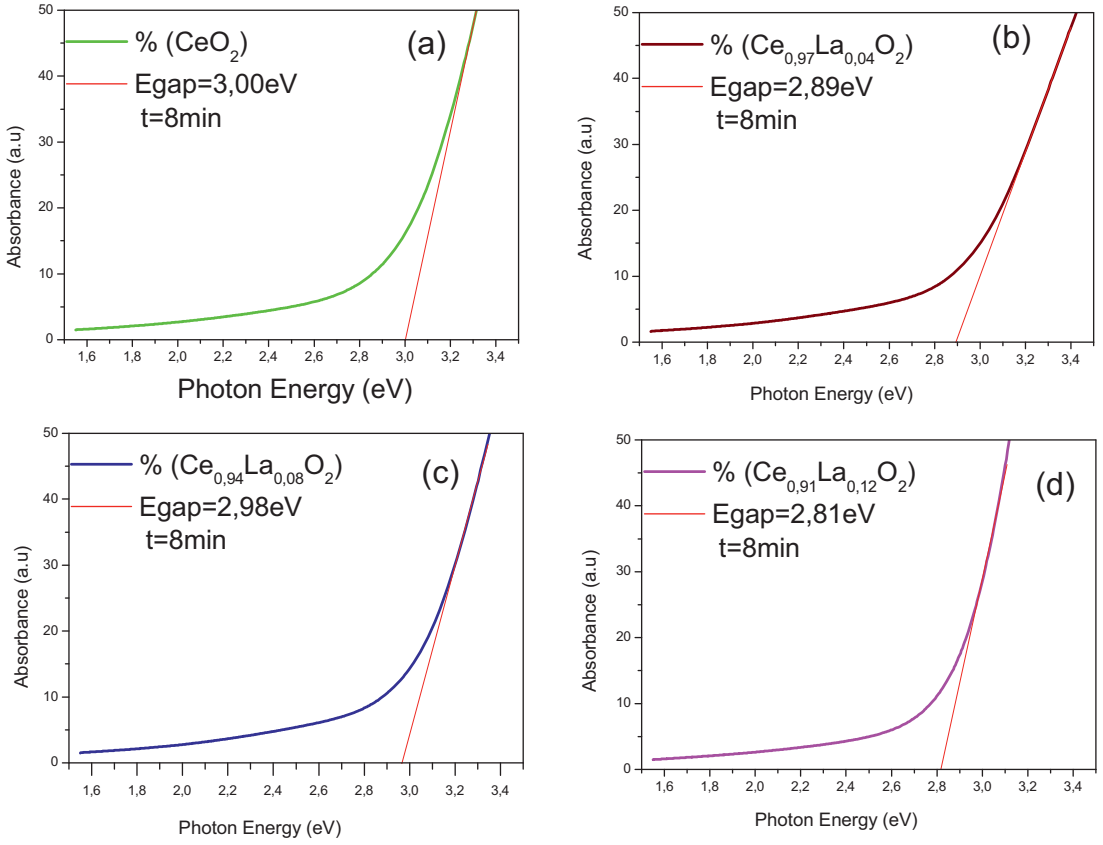

Fig. 6. UV–vis absorbance spectra of $Ce_{1-3/4x}La_xO_2$ nanoparticles synthesized at 100 °C in the MAH method under KOH mineralizer at different contents: (a) 0.00; (b) 0.04; (c) 0.08 and (d) 0.12.

levels in the band gap. The decrease in the band-gap of the La doped CeO_2 nanoparticles can be attributed to defects and/or local bond distortion, which yield localized electronic levels in the band-gap of this material. The irregularities in the optical band gap values can be related with the different preparation methods, shape, average crystal size and structural order–disorder degree in the lattice.

Fig. 7 shows the PL spectra of CeO_2 nanoparticles synthesized by MAH at 100 °C for 8 minutes as a function of La content. Whatever the sample, band at 610 nm became more intense as particle size was increased by hydrothermal treatment. As a consequence these bands may be attributed to bulk energy levels. This is consistent with their attribution to charge transfer (CT) transitions between O^{2-} and Ce^{4+} [47]. The PL emission is strongly dependent on the La content, due its addition causes changes in the defects or disorder of materials which affects the particle size. Two main mechanisms can be used to explain the PL of such particles. The first taking into account the main difference between the samples under hydrothermal ripening was their crystal growth: very weak for a higher particle size, significant for a lower particle size. As a consequence this band may be attributed to surface specific defects that disappear during growth under hydrothermal conditions. The second mechanism is clearly observed in the highest doped CeO_2 nanoparticles. The polycrystalline samples present two peaks: at 490 nm (blue–green emission) and the other at 610 nm (green emission). This behavior is likely associated with the structure organization level and the charge transfer occurring between oxygen and cerium ions. As lanthanum content increases more oxygen vacancies are produced affecting the whole particle size, as in agreement with TEM images. The characteristic photoluminescence peaks in the UV band are observed due to direct recombination of electrons in Ce 4f conduction band with holes in O 2p valence band, while the broad visible emission band has been suggested due to the presence of many point defects, such as oxygen vacancies. In the hydrothermal synthesis of CeO_2, the formation of crystal nuclei of its nanostructures begins when the concentration of CeO_2 reaches supersaturation, and generally, the faces perpendicular to the fast direction of growth have smaller surface areas and the faces whose normal directions correspond to slow growing ones thus dominate the final morphology [19,48–50]. It is noteworthy that these defects systematically exist in particles obtained by room temperature precipitation, whatever the pH, pressure and particle size are predominant. Interestingly, some cerium oxide particles directly synthesized in hydrothermal conditions did exhibit PL bands at 370 and 414 nm without significant emission at 460 nm [51], confirming that the intense peak at 460 nm was highly dependent from preparation processes. Intensity of PL emission changes with the increase of La content which is associated with structural disorganization level, and the charge transfer occurring between cerium, lanthanum and oxygen ions. As the lanthanum content increase, a significant raise in the particle size is observed which allows faster recombination of electrons in Ce 4f and La 3d conduction bands with holes in O 2p valence band increasing PL signal. However, it is very important to emphasize that at this condition no electronic levels of the amorphous [CeO_8] and [LaO_8] clusters included in the wideband gap of the crystalline cluster were evidenced. This conclusion is a good indication that the PL of CeO_2 powders obtained by the MAH

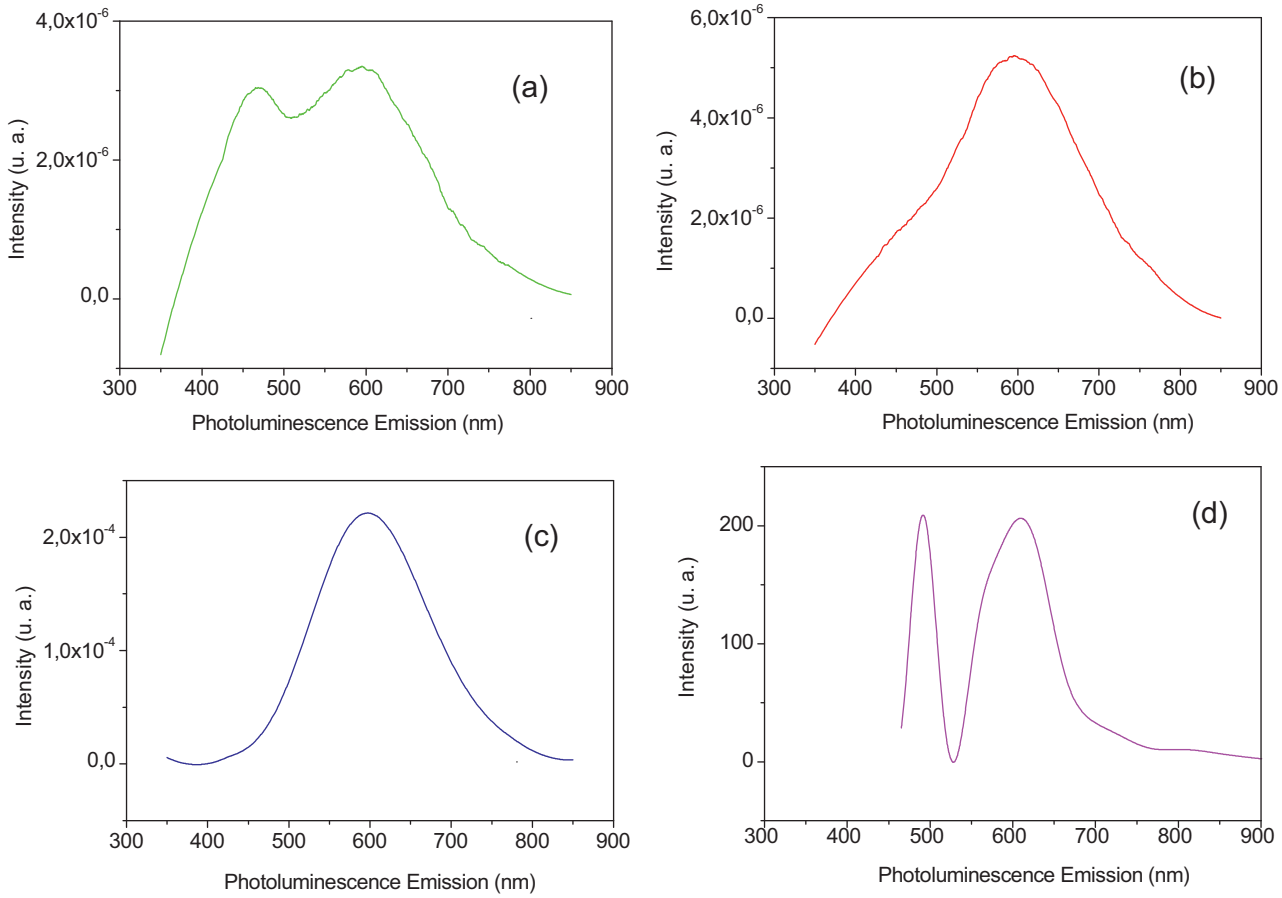

Fig. 7. PL spectra at room temperature of $Ce_{1-3/4x}La_xO_2$ nanoparticles synthesized at 100 °C in the MAH method under KOH mineralizer at different contents: (a) 0.00; (b) 0.04; (c) 0.08 and (d) 0.12.

originates from intrinsic defects and charge transfer after a certain degree of structural order. Probably, the PL of these powders is arising from the contribution of different intermediary energy levels within the band gap. This behavior is not associated to the band-to-band emission process due to the wavelength's energy (2.54 eV) to be small than the E_g of CeO_2 nanoparticles. Our results indicate that the CeO_2 nanoparticles processed in MAH are highly crystalline and structurally ordered at long and short range, in agreement with XRD patterns (Fig. 1). Therefore, PL of these powders is not due to the structural order–disorder in the lattice. As previously described, we believe that the behavior of this physical property is related to the influence of microwave radiation on the [CeO_8] octahedron groups. We believe that the interaction between microwave radiation and cerium groups results in a rapid heating and leads to a vibration on the charged particles. These factors probably result in a distortion process on the [CeO_8] and [LaO_8] octahedron groups, favoring the formation of intermediary energy levels within the band gap of this material. These energy levels are composed of oxygen 2p states (near the valence band) and lanthanum 3d states (below the conduction band). During the excitation process with 488 nm wavelength, some electrons are promoted from the oxygen 2p states to lanthanum 3d states through the absorption of photons ($h\nu$). This mechanism results in the formation of self-trapped excitons (STEs), i.e., trapping of electrons (e^-) by holes ($h^\bullet$). The emission process of photons ($h\nu$) occurs when an electron localized in a lanthanum 3d states decays into an empty oxygen 2p state. Consequently, this mechanism is responsible for the PL emission of CeO_2 nanoparticles. This proposed mechanism based on the distortion process of [CeO_8] and [LaO_8] octahedron groups consequently can be related with the non-linear variations on the PL intensity of CeO_2 nanoparticles with the La content. Also, this behavior can be associated with the formation of superficial defects caused by the modifications on the morphology of these powders [52]. These defects are arising from rapid heating, high effective collision rates between the small particles and growth processes during the processing of CeO_2 nanoparticles.

4. Conclusions

Adopting the microwave-hydrothermal process as synthesis method it is possible to obtain, by treating the solution at 100 °C, nanometric, crystalline and single phase ceria nanoparticles. As-prepared ceria powders crystallizes in a pure cubic structure of CeO_2 (space group: Fm3m) free of secondary phases. Raman scattering revealed with raising lanthanum content may reflect the increase of the oxygen vacancy concentration and absence of any other Raman mode suggesting pure cubic phase. Undoped CeO_2 nanoparticles obtained displays poor contrast and intense agglomeration amongst extremely fine particles while at higher La content aggregation between the particles decreases and monodispersed particles are observed. UV–vis spectra revealed that as La content increases, the optical band gap of the sample initially decreases and then increases because new levels of energy are formed promoting the appearance of intermediate electronic levels in the band gap. The mechanisms responsible for the PL emission of CeO_2 nanoparticles doped with La can be a consequence of emission process of photons ($h\nu$) when an electron localized in lanthanum 3d states decays into an empty oxygen 2p state and also affected by particle size during CeO_2 growth. MAH is important not only for the use of a short treatment time and low temperature but also for the possibility to control the morphological and structural properties. Therefore, the MAH method is undeniably a genuine technique for low temperatures and short times in comparison with the previous methodologies.

Acknowledgments

The financial support of this research project by the Brazilian research funding agencies CNPq 573636/2008-7, INCTMN 2008/57872-1 and FAPESP 2013/07296-2. We would like to thank Professor Elson Longo for facilities.

References

[1] C.B. Carter, M.G. Norton, Ceramic Materials: Science and Engineering, Springer, 2007.
[2] P. Jasinski, T. Suzuki, H.U. Anderson, Nanocrystalline undoped ceria oxygen sensor, Sens. Actuators B 95 (2003) 73–77.
[3] S. Park, J.M. Vohs, R.J. Gorte, Direct oxidation of hydrocarbons in a solid-oxide fuel cell, Lett. Nat. 404 (2000) 265–270.
[4] T. Meng, M. Ara, L. Wang, R. Naik, K.Y. Simon, Enhanced capacity for lithium–air batteries using $LaFe_{0.5}Mn_{0.5}O3$–CeO_2 composite catalyst, J. Mater. Sci. 49 (2014) 4058–4066.
[5] X.J. Yu, P.B. Xie, Q.D. Su, Size-dependent optical properties of nanocrystalline CeO_2: Er obtained by combustion, Phys. Chem. Chem. Phys. 3 (2003) 5266–5269.
[6] K. Chen, D. Xue, In-situ electrochemical route to aerogel electrode materials of graphene and hexagonal CeO_2, J. Colloid Interface Sci. 446 (2015) 77–83.
[7] A. Trovarelli, Properties of ceria and CeO_2- containing materials, catalysis reviews, Sci. Eng. 38 (1996) 439–520.
[8] C.W. Raubach, L. Polastro, M.M. Ferrer, A. Perrin, C. Perrin, A.R. Albuquerque, P. G.C. Buzolin, J.R. Sambrano, Y.B.V. de Santana, J.A. Varela, E. Longo, Influence of solvent on the morphology and photocatalytic properties of ZnS decorated CeO_2 nanoparticles, J. Appl. Phys. 115 (2014) 213514.
[9] B.M. Reddy, P. Bharali, P. Saikia, Structural characterization and oxide hydrogenation activity of CeO_2/Al_2O_3 and $V_2O_5/CeO_2/Al_2O_3$ Catalysts, J. Phys. Chem. C 111 (2007) 18751–18758.
[10] X. Lua, X. Li, F. Chen, C. Ni, Z. Chen, Hydrothermal synthesis of prism-like mesocrystal CeO_2, J. Alloys Compd. 476 (2009) 958–962.
[11] B. Djuricic, S. Pickering, Nanostructured cerium oxide: preparation and properties of weakly-agglomerated powders, J. Eur. Ceram. Soc. 19 (1999) 1925–1934.
[12] S. Dikmen, P. Shuk, M. Greenblatt, H. Gocmez, Hydrothermal synthesis and properties of $Ce_{1-x}Gd_xO_2$, Solid State Sci. 4 (2002) 585–590.
[13] S.W. Zha, C.R. Xia, G.Y. Meng, Effect of Gd (Sm) doping on properties of ceria electrolyte for solid oxide fuel cells, J. Power Sources 115 (2003) 44–48.
[14] Y.R. Wang, T. Mori, J.G. Li, T. Ikegami, Low-temperature synthesis of praseodymium-doped ceria nanopowders, J. Am. Ceram. Soc. 85 (2002) 3105–3107.
[15] R.C. Deus, M. Cilense, C.R. Foschini, M.A. Ramirez, E. Longo, A.Z. Simões, Influence of mineralizer agents on the growth of crystalline CeO. sub. 2 nanospheres by the microwave-hydrothermal method, J. Alloys Compd. 550 (2013) 245–251.
[16] C.S. Ricardi, R.C. Lima, M.L. Dos Santos, P.R. Bueno, J.A. Varela, E. Longo, Preparation of CeO_2 by a simple microwave–hydrothermal method, Solid State Ionic 118 (2009) 288–291.
[17] D. Zhang, X. Du, L. Shia, R. Gao, Shape-controlled synthesis and catalytic application of ceria nanomaterials, Dalton Trans. 41 (2012) 14455.
[18] E. Wuilloud, B. Delley, W.D. Schneider, Y. Baer, Spectroscopic evidence for localized and extended f-symmetry states in CeO_2, Phys. Rev. Lett. 53 (1984) 203–205.
[19] C. Sun, D. Xue, Size-dependent oxygen storage ability of nano-sized ceria, Phys. Chem. Chem. Phys. 15 (2013) 14414.
[20] S. Wang, K. Maeda, Direct formation of crystalline gadolinium-doped ceria powder via polymerized precursor solution, J. Am. Ceram. Soc. 85 (2002) 1750–1752.
[21] D.J. Kim, Lattice-parameters, ionic conductivities, and solubility limits in fluorite-structure $Hf^{4+}O_2$, $Zr^{4+}O_2$, $Ce^{4+}O_2$, $Th^{4+}O_2$, $V^{4+}O_2$ Oxide Solid-Solutions, J. Am. Ceram. Soc. 72 (1989) 1415–1421.
[22] S.J. Hong, A.V. Virkar, Lattice-parameters and densities of rare-earth-oxide doped ceria electrolytes, J. Am. Ceram. Soc. 72 (1995) 433–439.
[23] J.G. Li, T. Ikegami, T. Mori, T. Wada, Reactive $Ce_{0.8}RE_{0.2}O_{1.9}$ (RE = La, Nd, Sm, Gd, Dy, Y, Ho, Er, and Yb) powders via carbonate coprecipitation synthesis and characterization, Chem. Mater. 13 (2001) 2921–2927.
[24] D.P. Fagg, J.C.C. Abrantes, D. Perez-Coll, P. Nuñez, V.V. Kharton, J.R. Frade, The effect of cobalt oxide sintering aid on electronic transport in $Ce_{0.80}Gd_{0.20}O_{2-\delta}$ electrolyte, Electrochim. Acta 48 (2003) 1023–1029.
[25] W. Huang, P. Shuk, M. Greenblatt, Hydrothermal synthesis and properties of $Ce_{1-x}Sm_xO_{2-x/2}$ and $Ce_{1-x}Ca_xO_{2-x}$ solid solutions, Chem. Mater. 9 (1997) 2240–2245.
[26] W. Huang, P. Shuk, M. Greenblatt, Hydrothermal synthesis and properties of terbium- or praseodymium-doped $Ce_{1-x}Sm_xO_{2-x/2}$ solid solutions, Solid State Ion 113 (1998) 305–310.
[27] S. Dikmen, P. Shuk, M. Greenblatt, Hydrothermal synthesis and properties of $Ce_{1-x}Bixo_{2-\delta}$ solid solutions, Solid State Ion 112 (1998) 299–307.
[28] S. Dikmen, P. Shuk, M. Greenblatt, Hydrothermal synthesis and properties of $Ce_{1-x}La_xO_{2-}\delta$ solid solutions, Solid State Ion 126 (1999) 89–95.

[29] S. Dikmen, P. Shuk, M. Greenblatt, H. Gocmez, Hydrothermal synthesis and properties of $Ce_{1-x}La_xO_{2-\delta}$ solid solutions, Solid State Sci. 4 (2002) 585–590.
[30] R.D. Shannon, C.T. Prewitt, Revised effective ionic radii and systematic studies of interatomie distances in halides and chaleogenides, Acta Cryst. Section A 32 (1976) 751–767.
[31] D.G. Stroppa, C.J. Dalmaschio, L. Houben, J. Barthel, L.A. Montoro, E.R. Leite, A.J. Ramirez, Analysis of dopant atom distribution and quantification of oxygen vacancies on individual Gd- doped CeO_2 nanocrystals, Chem. Eur. J. 20 (2014) 6288–6293.
[32] B.C.H. Steele, Appraisal of $Ce_{1-y}GdyO_{2-y/2}$ electrolytes for IT-SOFC operation at 500 °C, Solid State Ionics 129 (2000) 95–110.
[33] M. Palard, J. Balencie, A. Maguer, J. Hochepied, Effect of hydrothermal ripening on the photoluminescence properties of pure and doped cerium oxide nanoparticles, Mater. Chem. Phys. 120 (2010) 79–88.
[34] T. Miki, M. Haneda, N. Kakuta, A. Ueno, S. Tateishi, S. Matsuura, M. Sato, Enhanced oxygen storage capacity of cerium oxides in $CeO_2/La_2O_3/Al_2O_3$, containing precious metals, J. Phys. Chem. 94 (1990) 6464–6468.
[35] S. Liang, E. Broitman, Y. Wang, A. Cao, G. Veser, Highly stable, mesoporous mixed lanthanum–cerium oxides with tailored structure and reducibility, J. Mater. Sci. 46 (2011) 2928–2937.
[36] R.F. Gonçalves, Photoluminescence and adsorption of CO_2 in $CaTiO_3$ nanoparticles doped with lanthanum, New Chem. 27 (2004) 862–865.
[37] H.M. Rietveld, A profile refinement method for nuclear and magnetic structures, J. Appl. Crystallogr. 2 (1939) 65–71.
[38] A.C. Larson, R.B. Von Dreele, Los Alamos National Laboratory Report No. LAUR 86-748, (2004).
[39] E. Kumar, P. Selvarajan, D. Muthuraj, Preparation and characterization of polyaniline/cerium dioxide (CeO_2) nanocomposite via in situ polymerization, J. Mater. Sci. 47 (2012) 7148–7156.
[40] H.R. Tan, J.P.Y. Tan, C. Boothroyd, Y.L. Hansen, M.J. Lin, Experimental evidence for self-assembly of CeO_2 particles in solution. formation of single-crystalline porous CeO_2 nanocrystals, J. Phys. Chem. C 116 (2012) 242–247.
[41] A.B. López, I.S. Basáñez, C.S.M. Lecea, Stabilization of active Rh_2O_3 species for catalytic decomposition of N_2O on La-, Pr-doped CeO_2, J. Catal. 244 (2006) 102–112.
[42] G. Reddy, Structural characteristics and catalytic activity of nanocrystalline ceria-praseodymia Solid Solutions, J. Phys. Chem. C 113 (2009) 15882.
[43] J.R. McBride, K.C. Hass, B.D. Poindexter, W.H. Weber, Raman and X-ray studies of $Ce_{1-x}RE_xO_{2-y}$, where RE = La, Pr, Nd, Eu, Gd, and Tb, J. Appl.Phys. 76 (1994) 2435.
[44] Z.Y. Pu, J.Q. Lu, M.F. Luo, Y.L. Xie, Study of oxygen vacancies in $Ce_{0.9}Pr_{0.1}O_{2-}$delta solid solution by in situ X-ray diffraction and in situ Raman spectroscopy, J. Phys. Chem. C (2007) 18695.
[45] G.J. Wilson, A.S. Matijasevich, D.R.G. Mitchell, J.C. Schulz, G.D. Will, Modification of TiO_2 for enhanced surface properties: finite ostwald ripening by a microwave hydrothermal process, Langmuir 22 (2006) 2016–2027.
[46] H. Wang, J.J. Zhu, J.M. Zhu, X.H. Liao, S. Xu, T. Ding, Preparation of nanocrystalline ceria particles by sonochemical and microwave assisted heating methods, Phys. Chem. 4 (2002) 3794–3799.
[47] Y.W. Zhang, S. Rui, C.S. Liao, C.H. Yan, Fe doped CeO_2 nanoparticles, J. Phys. Chem. B 107 (2003) 10159–10163.
[48] C. Sun, D. Xue, Physical chemistry of crystalline $(K,NH_4)H_2PO_4$ in aqueous solution: an in situ molecule vibration spectral observation of the early formation stage, J. Phys. Chem. C 118 (2014) 16043–16050.
[49] C. Sun, D. Xue, In situ IR spectral identification of $NH_4H_2PO_4$ structural evolution during crystallization in water-ethanol mixed solvent, Cryst. Eng. Commun. 17 (2015) 2728–2736.
[50] C. Sun, D. Xue, Chemical bonding theory of single crystal growth and its application to ϕ 3″ YAG bulk crystal, Cryst. Eng. Commun. 16 (2014) 2129–2135.
[51] M. Hirano, M. Inagaki, Preparation of monodispersed cerium (IV) oxide particles by thermal hydrolysis: influence of the presence of urea and Gd doping on their morphology and growth, J. Mater. Chem. 10 (2000) 473–477.
[52] B.P. Falcão, J.P. Leitão, M.R. González, C.F. Correia, A.G. de Oliveira, F.M. Zayas-Bazán, M.B. Moreira, Photoluminescence study of GaAs thin films and nanowires grown on Si(111), J. Mater. Sci. 48 (2013) 1794–1798.